Generalized Gross-Pitaevskii Equation for 2D Bosons with Attractive Interactions

Michał Suchorowski, 1, * Fabian Brauneis, Hans-Werner Hammer, 2, 3 Michał Tomza, 1 and Artem G. Volosniev^{4,†}

¹ Faculty of Physics, University of Warsaw, Pasteura 5, 02-093 Warsaw, Poland ² Department of Physics, Technische Universität Darmstadt, 64289 Darmstadt, Germany ³ Extreme Matter Institute EMMI and Helmholtz Forschungsakademie Hessen für FAIR (HFHF), GSI Helmholtzzentrum für Schwerionenforschung GmbH, 64291 Darmstadt, Germany ⁴ Center for Complex Quantum Systems, Department of Physics and Astronomy, Aarhus University, Ny Munkegade 120, DK-8000 Aarhus C, Denmark (Dated: November 14, 2025)

We introduce and investigate a generalized Gross-Pitaevskii equation for two-dimensional (2D) attractive Bose systems. First, we demonstrate that it accurately captures key properties of universal bound states in free space commonly referred to as quantum droplets. We then apply the framework to predict the existence of universal excited states, including vortex configurations, which may be more accessible to experimental investigation than the ground state. Additionally, we investigate breathing modes and quench dynamics in trapped geometries. Our results establish a robust theoretical foundation for exploring both static and dynamical phenomena in finite 2D Bose systems, offering guidance for the design of future experimental protocols.

Scale invariance of the attractive two-dimensional (2D) Gross-Pitaevskii equation (GPE) gives rise to unique phenomena such as Townes solitons [1], 'strong' self-similar collapse [2, 3], and interaction-independent breathing-mode frequencies in tightly trapped systems [4, 5]. In realistic systems of bosons, this symmetry is, however, broken by the presence of microscopic interactions that support bound states. It is now well established that these systems exhibit a strong quantum anomaly namely, a breaking of scale invariance [6] – one of whose most striking consequences is the formation of universal droplets (i.e., many-body bound states) [7]. Despite this exciting progress in our understanding of 2D attractive bosons, it remains unclear whether a simple, unified theoretical framework exists to analyze these phenomena. Consequently, each new solution represents a state-of-the-art effort; see, for example, recent studies in Refs. [8-10].

Here, to address this issue, we incorporate a density-dependent coupling strength into the GPE. The resulting equation successfully describes the behavior of universal droplets [7, 8], while preserving a simple structure suitable for intuitive analytical and numerical exploration. We demonstrate the power of the generalized GPE by examining universal vortex states, discussing breathing dynamics in a trap, and investigating quench dynamics near the trap-induced transition.

We note in passing that the mathematical treatment of 2D bosons shares conceptual similarities with the strong interaction in particle physics. Indeed, Quantum Chromodynamics (QCD) is asymptotically free [11, 12] and thus naively scale invariant at high energies, but this scale invariance is anomalous and broken by dimensional transmutation. In finite density QCD, a density-dependent coupling constant enters naturally [13], although in practice, the chemical potential is often used instead of the density [14]. Vortices in quark matter have also been con-

sidered [15, 16]. Our methods and results may be useful for building intuition about such QCD systems.

Framework. We study an ultradilute system of N 2D bosons with coordinates $\{\mathbf{x}_i\}$ and a mass m in a trap with the Hamiltonian

$$H = \sum_{i=1}^{N} \left(-\frac{\hbar^2}{2m} \frac{\partial^2}{\partial \mathbf{x}_i^2} + W(\mathbf{x}_i) \right) + \frac{1}{2} \sum_{i,j=1}^{N} V(\mathbf{x}_i - \mathbf{x}_j), (1)$$

where V describes short-range particle-particle interactions, and W is the trapping potential. To facilitate a clear and consistent illustration of our results, we either consider a free system (W=0) or employ a harmonic trap, $W(\mathbf{x}_i) = m\omega^2\mathbf{x}_i^2/2$.

In our analysis focused on the limit $N \gg 1$, we rely on the following approximation for the energy

$$\frac{E_N[\psi]}{N} = \int d\mathbf{x} \psi^* \left[-\frac{\hbar^2}{2m} \frac{\partial^2}{\partial \mathbf{x}^2} + W(\mathbf{x}) + \frac{gN}{2} |\psi|^2 \right] \psi, \tag{2}$$

where $\psi=\psi(\mathbf{x})$ is a normalized function ($\|\psi\|=1$) found by minimization of E_N . In what follows, we use the units with $\hbar=m=\omega=1$. Energy is then expressed in the units of $\hbar\omega$; interaction strength, g, in \hbar^2/m ; length in $\sqrt{\hbar/(m\omega)}$; time and frequencies in $1/\omega$ and ω , respectively. We will also often express length in the units of the state size, $R=\sqrt{\sum_i \langle \mathbf{x}_i^2 \rangle}/N$, which is the only relevant length scale in the regime of strong attractions.

A unique aspect of 2D many-boson systems is that their theoretical description requires the coupling constant g to depend on the system's probability density, $n=|\psi|^2$, even in the low-energy (i.e., weakly-interacting) regime. For repulsive boson-boson interactions V>0, a widely used expression is $g=4\pi/|\ln(Nna^2)|$ [17–19], where a denotes the 2D scattering length. The logarithmic dependence of g on n is notably weak, which poses challenges for experimental detection [6, 20]. Nevertheless, this density dependence has a fundamental impact

– it underlies the aforementioned symmetry breaking, as the scale invariance of the mean-field approximation relies on the assumption that g remains constant.

For attractive interactions and in the absence of an external potential (W=0), a possible form of the coupling constant is $g \simeq -4\pi/|\ln(R^2B_2)|$ [7], where $B_2 > 0$ denotes the two-body binding energy. This expression is, however, not as practically useful as the one for repulsive interactions. In particular, it cannot be straightforwardly extended to include an external trap – essential for modeling cold-atom systems – since the parameter R must then be determined from a separate equation, which is challenging to solve numerically [10]. Furthermore, it is unclear how to use this coupling constant in time-dependent problems. In what follows, we propose a modified form of q that circumvents these limitations.

Coupling constant. For W=0, the bosonic system forms a droplet whose size, R^2 , is exponentially smaller than that of the corresponding two-body bound state, characterized by $1/B_2$ [7]. Consequently, the coupling g in free space is mainly determined by the value of R^2 .

The R is the only length scale of the many-body problem that determines the properties of the droplet, e.g., its density is given by $N|\psi|^2 \sim F(r/R)^2/R^2$, where $r=|\mathbf{x}|$; F denotes a universal function that captures the shape of the droplet. The exponential dependence of the parameter R on N and the fact that the amplitude of the function ψ is given by 1/R motivates the following ansatz for g in the limit $N\gg 1$

$$g \simeq -\frac{4\pi}{\ln\left(\alpha|\psi(\mathbf{x})|^2/B_2\right)},\tag{3}$$

where $\alpha=2.607$. Our choice of the parameter α is fixed by the ground state energy derived in Ref. [8], as described in the Supplemental Material (SM) [21]. For W=0, Eq. (3) is (within logarithmic accuracy) equivalent to $-4\pi/|\ln(R^2B_2)|$ derived in Ref. [7] everywhere except the points where $\psi(\mathbf{x})$ vanishes. This region, however, does not contribute to the energy functional in Eq. (2) where g is multiplied by $|\psi|^2$.

Although Eq. (3) is inspired by the strongly-interacting regime where the trap can be neglected, it remains a natural choice for weakly interacting systems in a trap, i.e., when $B_2 \to 0$. Indeed, in this case, the coupling constant obeys $g \simeq -4\pi/\ln(a^2)$, see, e.g., Ref. [9]. Within logarithmic accuracy, this expression coincides with Eq. (3) (recall that $B_2 \sim 1/a^2$, see, e.g., Ref. [22]). Finally, to assess the validity of Eq. (3) at intermediate interaction strengths, we perform numerical calculations as presented in Fig. 1, see the discussion below and SM [21]. [Intermediate interaction strengths correspond to $(\ln B_2)/N \simeq -2.15$ [23], see Refs. [9, 10] and below.]

Gross-Pitaevskii equation. Using Eq. (3) in Eq. (2) and the equation of motion $i\partial\psi/\partial t = \delta E[\psi]/\delta\psi^*$, we derive

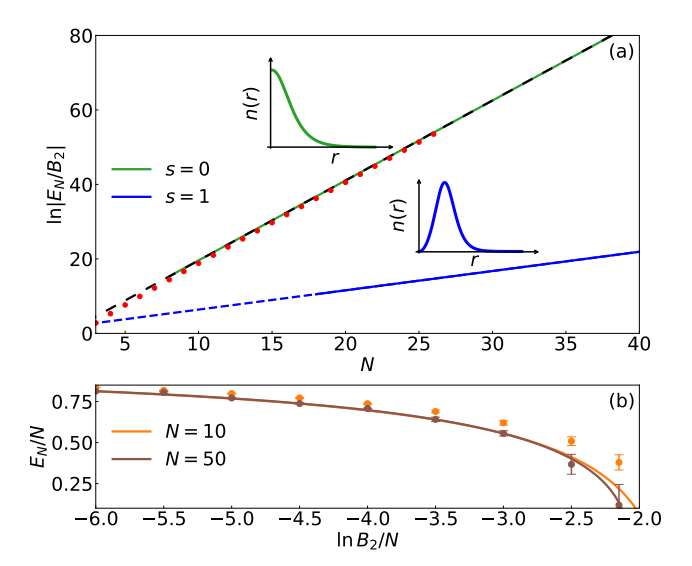


FIG. 1. (a) Energy, $\ln |E_N/B_2|$, as a function of the number of bosons N for the lowest energy states with s=0 and s=1 in the limit $W\to 0$. The solid green line shows numerical solution of Eq. (4) for s=0; the black dashed line shows the expected asymptote $\ln |E_N/B_2| = \frac{4\pi N}{\mathcal{G}} - 1.91$ [8]. The red dots demonstrate the numerically exact solution of Eq. (1) available for 'small' values of N [25]. The blue line shows the lowest energies for s=1. The blue dashed line is a linear fit to this result, $\ln |E_N/B_2| = 0.5174N + 1.218$. The insets sketch the radial densities for the states. (b) The lowest energy solution of Eq. (4) for weak/intermediate interactions (solid lines) together with the numerical solution to Eq. (1) obtained using flow equations for bosons (dots with error bars).

the generalized Gross-Pitaevskii equation

$$i\frac{\partial \psi}{\partial t} = \left[-\frac{1}{2} \frac{\partial^2}{\partial \mathbf{x}^2} + W(\mathbf{x}) + GN|\psi|^2 \right] \psi, \tag{4}$$

where $G=g+g^2/(8\pi)$ [24]. Equation (4) provides a powerful framework that greatly facilitates the analysis of 2D systems with attractive interactions. To illustrate this, we first calculate static properties of the system, i.e., we solve Eq. (4) in polar coordinates using the ansatz $\psi(\mathbf{x},t)=e^{-i\mu t}e^{is\phi}\sqrt{n(r)}$, where μ is the chemical potential, and the topological quantum number s determines the vorticity of the system.

Universal states without a trap. Given a logarithmic dependence of G on $\psi(\mathbf{x})$, we gain analytical insight into the equilibrium properties of Eq. (4) by treating G as constant. Under this assumption, Eq. (4) with W=0 is stable only for specific values of $GN=\mathcal{G}<0$, where \mathcal{G} is independent of N [26]. These values correspond to the fixed points of the energy functional in Eq. (2), where the function ψ has the form $\psi \sim e^{is\phi}F_{\mathcal{G},s}(r/R)/R$, here $F_{\mathcal{G},s}$ is a universal function parametrized by \mathcal{G} and s. The associated length scale follows from Eq. (3) for $N\gg 1$: $R^2\simeq 1/B_2e^{4\pi N/\mathcal{G}}$.

The smallest possible $|\mathcal{G}|$, $\mathcal{G} \simeq -5.84$, determines the ground state, whose static properties are by now well established [7, 8]. Within our framework, these properties can be readily studied numerically using Eq. (4) [27], see Fig. 1. Beyond the ground state, the generalized Gross-Pitaevskii equation also predicts the existence of universal excited states in the energy spectrum of Eq. (1). These states are connected to the spectrum of solutions to the 2D Gross-Pitaevskii equation, either without [28] or with vorticity [29] (see Ref. [26] for a review).

To illustrate one such state, we consider the vortex solution. Specifically, Fig. 1 presents the energy of the lowest-energy configuration with topological charge s=1. This solution corresponds to a critical interaction strength of $\mathcal{G}\simeq -24.15$. The energies of the corresponding states are $E_N^e\sim 1/R^2$; they lead to the universal scaling relation $E_{N+1}^e/E_N^e\simeq 1.7$, which may be contrasted with the ground-state scaling $E_{N+1}^g/E_N^g\simeq 8.6$ [7]. Note the markedly slower increase in energy with growing particle number – a distinctive trait of the excited-state spectrum. This suggests that topologically protected excited states can be more suitable for the experimental observation of 2D universality than the ground state.

Benchmarking Eq. (4) at intermediate interactions. One potential experimental platform for observing universal states is a trapped ultracold atomic gas [30]. To inform this effort, the influence of the trapping potential on universal states should be systematically investigated, which becomes possible using Eq. (4). We start by benchmarking the ground-state energy of Eq. (4) with a trap against the corresponding numerical result for Eq. (1), see Fig. 1(b). Our focus is on weak and intermediate interaction strengths, i.e., when |GN| is smaller than $|\mathcal{G}|$, which leads to $\ln B_2/N \lesssim 4\pi/\mathcal{G} \simeq -2.15$.

To solve Eq. (1) numerically, we employ the flowequation approach [31, 32] in the specific form developed for degenerate Bose systems [21, 33]. The overall agreement between the data in Fig. 1(b) is good (see SM [21] for the corresponding densities), further validating the applicability of the generalized GPE. Note that the agreement between the results is better for N=50than for N = 10. This behavior, which mirrors the strongly interacting limit – see the difference between the red dots and the solid green line in Fig. 1 – is expected. Our parametrization of the interaction strength, particularly the numerical value of α , explicitly relies on the assumption that $N \gg 1$. Nevertheless, the discrepancy is already marginal at $N \sim 10$ and does not affect our main conclusions. Finally, we remark that Fig. 1 shows the first application of the flow equations introduced in Refs. [33, 34] to 2D systems, paving the way for their exploration in three dimensions.

Effect of the trap on universal states. To further investigate the effect of the trap, we solve Eq. (4) (see SM [21] for numerical method details). In the weakly interacting regime $(B_2 \to 0)$, the density is predominantly shaped

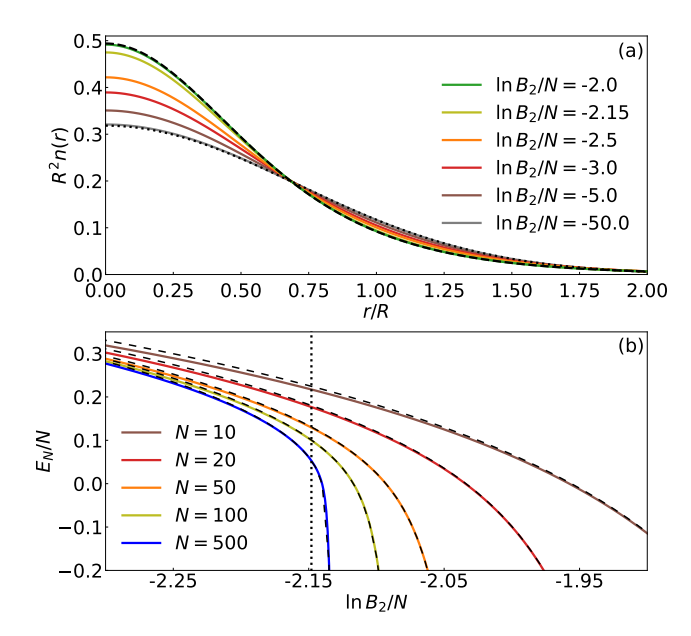


FIG. 2. (a) The density profile in the transition between the weakly- and strongly-interacting limits. The dimensionless density, $R^2n(r)$, for the ground state with s=0 and N=50 is plotted as a function of r/R for different interaction strengths $\ln B_2/N$. The dotted black line shows the non-interacting harmonic oscillator solution, and the dashed line represents the Townes-soliton profile. (b) Energy, E_N , as a function of the interaction parameter $\ln B_2/N$. The solid curves show the exact numerical result, the dashed black curves present the result of minimization with respect to the Townes-soliton profile. Different curves correspond to different numbers of particles. The vertical dotted line shows the transition point in the limit $N \to \infty$ [9, 10].

by the trapping potential. In contrast, for strong interactions $(B_2 \to \infty)$, the universal (so-called Townes soliton [1]) profile is expected to emerge. Figure 2(a) illustrates the transition between these two limits. The rescaled density exhibits a crossover behavior, with only a weak dependence on the interaction strength [35].

It is important to note that the generalized Gross-Pitaevskii equation admits solutions for all finite values of B_2 and N, in contrast to the standard GPE, which exhibits mass concentration (collapse) as the interaction strength approaches a critical value from below [36]. In our case, this unphysical behavior is replaced by a smooth increase in energy [37], which becomes more pronounced near a critical value of the parameter $\ln B_2/N \simeq -2.15$, as shown in Fig. 2(b). The derivative of the energy also varies smoothly (see SM [21]), suggesting a crossover rather than a sharp phase transition.

Breathing dynamics. The generalized Gross-Pitaevskii equation enables a quantitative description of the system using simple (semi-)analytical tools. For instance, in the challenging regime of intermediate interaction strengths, the system's energy can be obtained variationally by employing the Townes-soliton profile $f_{\rm T}(r/\tilde{R})$ where \tilde{R} is a

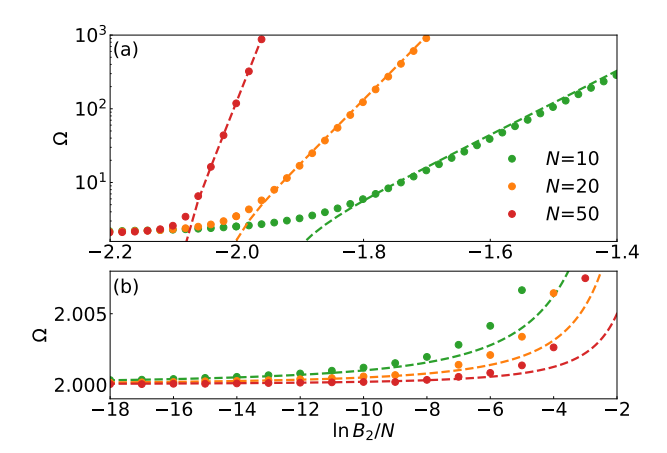


FIG. 3. Breathing mode frequencies Ω as a function of interaction strength $\ln B_2/N$ for different numbers of bosons N in (a) strong and (b) weak interaction regimes. Dots demonstrate frequencies from the numerical solutions. The dashed curves show analytical results valid for $N \gg 1$: (a) $3.8|E_N|/\sqrt{N}$; (b) $2 + N/(\ln B_2)^2$.

variational parameter that minimizes the mean-field energy (see Fig. 2(b) and SM [21]). As another illustrative example, we analyze breathing mode frequencies.

We perform this analysis in a harmonic trap, which enables us to compare and contrast with the known results for the standard Gross-Pitaevskii equation [4, 5]. To calculate breathing-mode frequencies, we first compute the time dynamics of $R^2 = \langle r^2 \rangle$ (see SM [21] for detailed derivation). The corresponding equation for large values of N is given by

$$\frac{\mathrm{d}^2 R^2}{\mathrm{d}t^2} = 4 \frac{E_N}{N} - 4R^2 + 2N \left\langle n^2 \frac{\mathrm{d}g}{\mathrm{d}n} \right\rangle. \tag{5}$$

This equation is general in the sense that it applies to any time dynamics of the state. For example, a time-independent problem requires $E_N = NR^2 - \frac{N^2}{2} \left\langle n^2 \frac{\mathrm{d}g}{\mathrm{d}n} \right\rangle$. Note that the total energy comprises two contributions: one from the harmonic confinement and another from density-dependent interactions. These contributions are balanced when $E_N = 0$, offering an intuitive explanation for the transition point between weakly and strongly interacting regimes, as illustrated in Fig. 2(b).

If g were a constant, the last term in Eq. (5) would disappear, resulting in interaction-independent dynamics governed solely by the first two terms [4, 5]. A density-dependent g breaks this picture, leading to a 'quantum anomaly', similar to dimensional transmutation in QCD [11, 12] or the Efimov effect [38, 39]. We investigate this phenomenon for the breathing dynamics, assuming that the solution has the form $\psi(r/R(t))/R(t)$. The time dynamics of R(t) follows from Eq. (5): $R^2(t) = 4E_N/N - 4R^2(t) + N\langle ng^2/2\pi\rangle/R^2(t)$, where the overline highlights that the expectation value is taken with respect to a re-scaled function $\psi(r)$. Looking for small

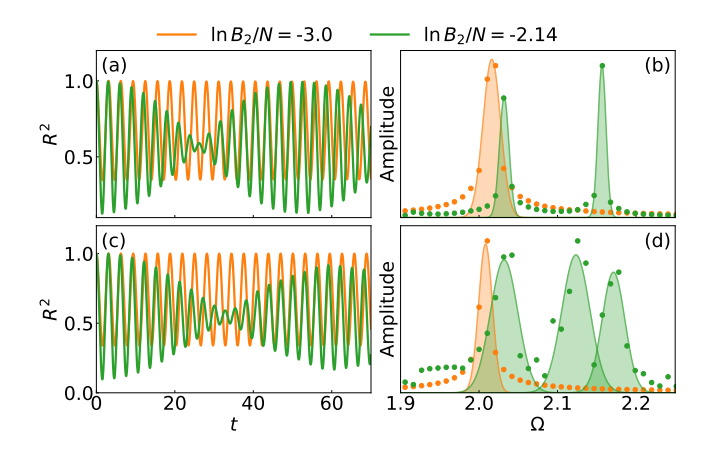


FIG. 4. Quench dynamics for systems with N=20 (a-b) and 50 (c-d) from a non-interacting system to the interaction strength $\ln B_2/N=-3.0$ and -2.14. Panels (a,c) demonstrate the size of the system, R^2 , as a function of time t. Panels (b,d) demonstrate the Fourier transforms of the R^2 signal (dots). To facilitate interpretation, we fit each peak with a Gaussian function (solid lines with shaded areas).

oscillations of R(t) in the vicinity of the equilibrium value R(t=0), we find the frequency of the breathing mode $(N\gg 1)$

$$\Omega = \sqrt{8 - 4E_N/(NR^2(t=0))},\tag{6}$$

where we have used the time-independent solution to Eq. (5). For weak interactions, Eq. (6) leads to $\Omega \simeq 2 + N/(\ln B_2)^2$. The deviation from the expected value $\Omega = 2$, characteristic of scale-invariant dynamics [4], underscores the presence of dynamics beyond those captured by the standard Gross-Pitaevskii equation. For strong interactions, the harmonic trap does not play a role, and Eq. (6) can be analyzed using the density of the Townes soliton, which leads to $\Omega \simeq 3.8|E_N|/\sqrt{N}$ in excellent agreement with recent calculations of Petrov [8], providing further support for our framework.

To illustrate the applicability of the derived expressions, we perform numerical analysis of breathing dynamics, see Fig. 3. To this end, we consider the time evolution of the system after a sudden change of the interaction from $\ln B_2/N$ to $\ln B_2/N - 0.001$. We see the transition between the two limits in the vicinity of $\ln B_2/N \simeq -2.15$ where the frequency of oscillations starts to rapidly increase. This transition becomes sharper as the number of particles increases reflecting the results presented in Fig. 2(b).

Quench dynamics. We anticipate that one of the main applications of the generalized Gross-Pitaevskii equation will be the exploration of non-equilibrium dynamics – an area that appears otherwise inaccessible for 2D attractive Bose gases. To illustrate this possibility, we consider the quench dynamics of the system—a standard paradigm for investigating non-equilibrium physics in closed sys-

tems [40]. We initiate the system in the ground state of the harmonic oscillator at t=0 and consider the time dynamics of $\langle r^2 \rangle$ at t>0, assuming a finite value of B_2 , see Fig. 4. We see that for weak interactions, the quench dynamics generates oscillations at frequencies $\Omega \simeq 2$, consistent with the scale-invariant dynamics. At stronger interactions, this universality breaks down, and we observe an interference pattern (beating) in the time evolution. This interference arises from the time dynamics of g in Eq. (5), which resonates with the universal, scale-invariant dynamics. By analyzing the frequencies of the ensuing modes, we gain insight into the system's excitation spectrum.

Summary and Outlook. In this Letter, we introduced and explored a non-linear equation for attractive 2D Bose systems, providing a bridge to the well-established mean-field description of repulsive interactions [19, 41, 42]. Our work motivates further mathematical and numerical studies to validate the proposed framework and identify experimental conditions for observing 2D universality in attractive systems. A concrete direction involves confirming the existence of excited states whose energies scale with the two-body binding energy [43], and exploring protocols for realizing such states—particularly universal vortex solutions whose slow energy increase with growing number of particles can present an experimental opportunity.

Note added: While completing our manuscript, we became aware of Refs. [44, 45], which discussed the exponential dependence of the ground-state energy on the number of bosons, independently from Ref. [7]. However, these works predict a different exponent compared to Ref. [7].

We thank Robert Seiringer for useful discussions and making us aware of Refs. [44, 45]. We thank Dmitry Petrov for enlightening correspondence. We gratefully acknowledge the National Science Centre, Poland (grants no. 2020/38/E/ST2/00564 and 2023/49/N/ST2/03820) for financial support and Poland's high-performance computing infrastructure, PLGrid (HPC Centers: ACK Cyfronet AGH), for providing computer facilities and support (computational grant no. PLG/2024/017527); A. G. V. acknowledges the support from Danish National Research Foundation through the Center of Excellence "CCQ" (DNRF152); H.-W. H. acknowledges the support by Deutsche Forschungsgemeinschaft (DFG, German Research Foundation) under Project ID 279384907 – SFB 1245, and by the German Federal Ministry of Education and Research (BMBF) (Grant No. 05P24RDB).

- Lett. 13, 479-482 (1964).
- V. E. Zakharov, Sov. Phys. JETP 35, 908 (1972).
- [3] V. E. Zakharov and E. A. Kuznetsov, Zh. Eksp. Teor. Fiz. 91, 1310 (1986).
- [4] L. Pitaevskii, Phys. Lett. A **221**, 14–18 (1996).
- [5] L. P. Pitaevskii and A. Rosch, Phys. Rev. A 55, R853–R856 (1997).
- [6] M. Olshanii, H. Perrin, and V. Lorent, Phys. Rev. Lett. 105, 095302 (2010).
- [7] H.-W. Hammer and D. T. Son, Phys. Rev. Lett. 93, 250408 (2004).
- [8] D. S. Petrov, SciPost Phys. 19, 037 (2025).
- [9] A. Tononi, G. E. Astrakharchik, and D. S. Petrov, AVS Quantum Sci. 6, 023201 (2024).
- [10] F. Brauneis, A. G. Volosniev, and H.-W. Hammer, Phys. Rev. A 111, 063308 (2025).
- [11] D. J. Gross and F. Wilczek, Phys. Rev. Lett. 30, 1343 (1973).
- [12] H. D. Politzer, Phys. Rev. Lett. 30, 1346 (1973).
- [13] J. C. Collins and M. J. Perry, Phys. Rev. Lett. 34, 1353 (1975).
- [14] A. Kurkela, P. Romatschke, and A. Vuorinen, Phys. Rev. D 81, 105021 (2010).
- [15] K. Iida and G. Baym, Phys. Rev. D 66, 014015 (2002).
- [16] M. Eto, M. Nitta, and N. Yamamoto, Phys. Rev. Lett. 104, 161601 (2010).
- [17] M. Schick, Phys. Rev. A 3, 1067–1073 (1971).
- [18] S. I. Shevchenko, Sov. J. Low Temp. Phys. 18, 223–230 (1992).
- [19] E. H. Lieb, R. Seiringer, and J. Yngvason, Commun. Math. Phys. 224, 17 (2001).
- [20] E. B. Kolomeisky, T. J. Newman, J. P. Straley, and X. Qi, Phys. Rev. Lett. 85, 1146–1149 (2000).
- [21] See Supplemental Material for (S1) description of our choice of the parameter α, (S2) additional information about the flow-equations method, (S3) description of the numerical method used to solve the extended GPE, (S4) additional information about variational data presented Fig. 2(b), (S5) derivative of the energy presented in Fig. 2(b) (S6) detailed derivation of Eq. (5). The Supplemental Material contains additional references [46–57].
- [22] J. Levinsen and M. M. Parish, Strongly interacting twodimensional Fermi gases, in *Annual Review of Cold Atoms and Molecules* (WORLD SCIENTIFIC, 2015) p. 1–75
- [23] $(\ln B_2)/N$ is a parameter that we shall use to quantify the interaction strength. For simplicity, we omit the parentheses in the numerator and write it simply as $\ln B_2/N$ in what follows.
- [24] It may be tempting to disregard the g^2 term due to its typically minor energy contribution, just as it is typically done for repulsive systems [42]. However, in finite systems and time-dependent scenarios, it is essential for preserving energy conservation.
- [25] B. Bazak and D. S. Petrov, New J. Phys. 20, 023045 (2018).
- [26] B. Bakkali-Hassani and J. Dalibard, in Proceedings of the International School of Physics "Enrico Fermi", Course 211 – Quantum Mixtures with Ultra-cold Atoms, edited by R. Grimm, M. Inguscio, and S. Stringari (IOS Press, Amsterdam, 2024).
- [27] In practice, calculations are performed in the presence of a very weak external potential, which enhances the stability of our numerical approach. See the Supplemen-

m.suchorowski@uw.edu.pl artem@phys.au.dk

^[1] R. Y. Chiao, E. Garmire, and C. H. Townes, Phys. Rev.

- tal Material for further information about the numerical method [21].
- [28] H. A. Haus, Appl. Phys. Lett. 8, 128–129 (1966).
- [29] V. Kruglov, Y. Logvin, and V. Volkov, J. Mod. Opt. 39, 2277–2291 (1992).
- [30] I. Bloch, J. Dalibard, and W. Zwerger, Rev. Mod. Phys. 80, 885–964 (2008).
- [31] S. Kehrein, *The Flow Equation Approach to Many-Particle Systems* (Springer Berlin Heidelberg, 2006).
- [32] K. Tsukiyama, S. K. Bogner, and A. Schwenk, Phys. Rev. Lett. 106, 222502 (2011).
- [33] A. G. Volosniev and H.-W. Hammer, New J. Phys. 19, 113051 (2017).
- [34] F. Brauneis, H.-W. Hammer, M. Lemeshko, and A. Volosniev, SciPost Phys. 11, 008 (2021).
- [35] This weak dependence stands in contrast to the behavior observed in a bubble trap [9], which features a transition from a uniform density to a localized droplet. In that case, the transition involves spontaneous symmetry breaking, potentially leading to dynamics that differ significantly from those presented here. The existence of a vanishing energy Bogoliubov mode in Eq. (4) for a bubble trap confirms this assertion. [For a homogeneous density, the Bogoliubov analysis can be performed as in Ref [9]].
- [36] Y. Guo and R. Seiringer, Lett. Math. Phys. 104, 141–156 (2013).
- [37] Collapse cannot occur in our 'asymptotically free' theory, because the coupling constant vanishes at high densities. In other words, the physics of the high-density regime is governed primarily by kinetic energy, which does not allow the system to collapse.
- [38] V. Efimov, Phys. Lett. B **33**, 563 (1970).
- [39] E. Braaten and H. W. Hammer, Phys. Rept. 428, 259 (2006).
- [40] A. Polkovnikov, K. Sengupta, A. Silva, and M. Vengalattore, Rev. Mod. Phys. 83, 863–883 (2011).
- [41] M. D. Lee and S. A. Morgan, J. Phys. B: At. Mol. Opt. Phys 35, 3009 (2002).
- [42] A. Y. Cherny and A. A. Shanenko, Phys. Rev. E 64, 027105 (2001).
- [43] Notably, it is already known that the 2D three-body (four-body) system supports a single excited state with zero angular momentum and energy $1.27B_2$ [58, 59] (25.1 B_2 [60]). According to Eq. (4) one could expect that the large-N limit for such excited states reads $B_2e^{4\pi N/|\mathcal{G}|}$, where $|\mathcal{G}|=38.6$ corresponds to the excited state of the generalized GPE with s=0. It is also plausible that these excited states are beyond the reach of our mean-field-like approach. Classifying such states in 2D attractive systems presents a compelling direction for future research.
- [44] S. G. Rajeev, A condensation of interacting bosons in two dimensional space (1999), arXiv:hep-th/9905120 [hepth].
- [45] S. G. Rajeev, Bound states in models of asymptotic freedom (1999), arXiv:hep-th/9902025 [hep-th].
- [46] Note that in many sources, including Ref. [8], \mathcal{R} is denoted as R, unlike the notation used in the main text of this Letter.
- [47] A. G. Volosniev and H.-W. Hammer, Phys. Rev. A 96, 031601 (2017).
- [48] F. Brauneis, T. G. Backert, S. I. Mistakidis, M. Lemeshko, H.-W. Hammer, and A. G. Volosniev, New J. Phys. 24, 063036 (2022).

- [49] F. Brauneis, A. Ghazaryan, H.-W. Hammer, and A. G. Volosniev, Commun. Phys 6, 224 (2023).
- [50] F. Brauneis, H.-W. Hammer, S. M. Reimann, and A. G. Volosniev, Phys. Rev. A 111, 013303 (2025).
- [51] W. Bao and Q. Du, SIAM J. Sci. Comput. 25, 1674 (2004).
- [52] X. Antoine and R. Duboscq, Comput. Phys. Commun. 185, 2969 (2014).
- [53] Y. Saad, *Iterative Methods for Sparse Linear Systems*, 2nd ed., Other Titles in Applied Mathematics (SIAM, 2003).
- [54] Krylovkit.jl, https://jutho.github.io/KrylovKit.jl (2022).
- [55] W. Bao and H. Wang, J. Comput. Phys. **217**, 612 (2006).
- [56] G. M. Koutentakis, S. I. Mistakidis, and P. Schmelcher, Atoms 10(1), 3 (2022).
- [57] M. Suchorowski, Julia Generalized GPE Solver for 2D Attractive Bose Gas (2025).
- [58] L. W. Bruch and J. A. Tjon, Phys. Rev. A 19, 425–432 (1979).
- [59] E. Nielsen, D. V. Fedorov, and A. S. Jensen, Few-Body Syst. 27, 15–55 (1999).
- [60] L. Platter, H.-W. Hammer, and U.-G. Meissner, Few-Body Syst., 169–174 (2004).

Supplemental Material

S1. PARAMETER α

To determine α in Eq. (3) from the main text, we first compute the energies of the system in the limit $W \to 0$, where according to Ref. [8] the ground state energy for $N \gg 1$ approaches $B_N^{s=0} \to B_2 e^{\frac{4N}{C} + c_1}$ with $C \simeq 1.862$ and $c_1 \simeq -1.91$. By trial and error, we found that $\alpha \simeq 2.607$ reproduces this limiting behavior well, see Fig. S1(b). Other values of α can be used if one finds this necessary. In particular, our model does not rule out the possibility for N-dependent α : $\alpha(N) = \alpha_0 + \alpha_1 N^{\gamma} + \ldots$. The inclusion of this N-dependence might be needed to describe the energy in the few-body limit accurately. Below, we outline the basic intuition behind determining the value of α that can be used for a further exploration of the generalized GPE.

In the limit $W \to 0$, $N \to \infty$, the wavefunction is well represented by the Townes soliton $\psi_{\rm T}(r) = (2\pi C \mathcal{R}^2)^{-1/2} f_{\rm T}(r/\mathcal{R})$, where $\mathcal{R}^2 = \frac{C}{M_2} \langle \psi_{\rm T} | r^2 | \psi_{\rm T} \rangle$ with $M_2 \simeq 2.211$ [46]. For more details about the Townessoliton profile $f_{\rm T}$, see Sec. S4. Therefore, the interaction strength in this limit should have the form

$$g = -\frac{4\pi}{\ln\left(\frac{\alpha(N)}{2\pi C}|f_{\rm T}|^2 \frac{1}{\mathcal{R}^2 B_2}\right)}.$$
 (S1)

We rewrite this expression at the fixed point of the generalized GPE (note that $G \simeq g$ in the considered limit):

$$\mathcal{G} \simeq -\frac{4\pi N}{\ln\left(\frac{\alpha(N)}{2\pi C} F_{\text{eff}} \frac{1}{\mathcal{R}^2 B_2}\right)},$$
 (S2)

where $\mathcal{G} = -\pi C$ and F_{eff} is a numerical constant representing some effective value of the density. System's energy is $E_N = -\frac{C}{8\mathcal{R}^2}$ (see, e.g., Ref. [8]) and therefore

$$\frac{E_N}{B_2} = -\frac{\pi C^2}{4} \frac{1}{\alpha(N)} \frac{1}{F_{\text{eff}}} e^{\frac{4N}{C}}.$$
 (S3)

Now, we propose that $F_{\text{eff}} = \kappa |f_{\text{T}}(0)|^2$ with scaling coefficient κ .

To determine κ and illustrate possible N dependence of α , we solve numerically Eq. (4) from the Main Text, for $\alpha(N) = N^{\gamma}$ with $\gamma = -1, 0, \frac{1}{2}, 1$. We use calculated values of E_N/B_2 and Eq. (S3) to fit the parameter $\kappa = 1.448$. Note that the parameter κ is independent of the $\alpha(N)$. In panel (a) and (c) of Fig. S1, we show $\ln |E_N/B_2|$ and E_{N+1}/E_N for different $\alpha(N)$ compared to Refs. [8, 25]. Panel (b) presents the difference $\Delta \ln |E_N/B_2| = \ln |E_N/B_2| - (4N/C + c_1)$ where E_N/B_2 comes from solution of generalized GPE and from Eq. (S3) with $\kappa = 1.448$.

Once the parameter κ is determined, we can estimate

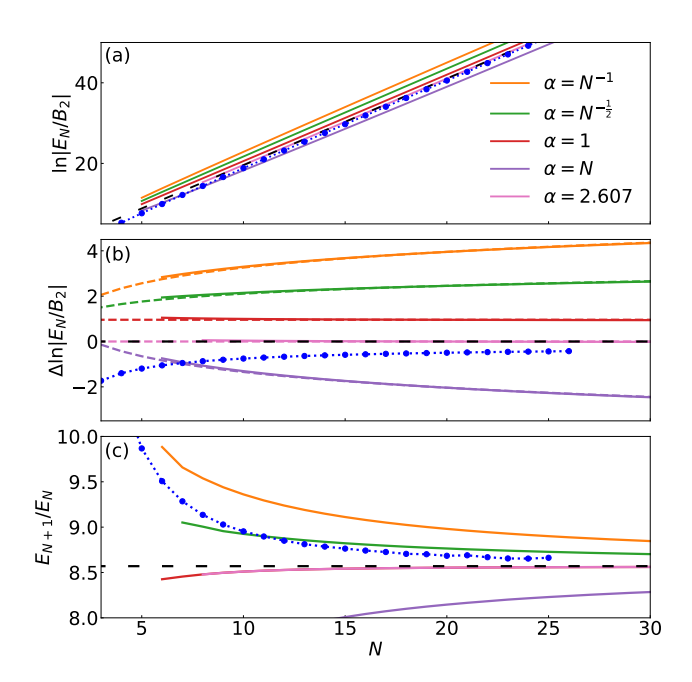


FIG. S1. (a) Energy $\ln |E_N/B_2|$, (b) energy difference to expected asymptote [8] $\Delta \ln |E_N/B_2| = \ln |E_N/B_2| - (4N/C + c_1)$, (c) energy ratio E_{N+1}/E_N for different $\alpha(N)$. Solid lines represent solutions of the generalized GPE. The black dashed line represents the solution of Ref. [8], and the blue dots with a dotted line show the results of Ref. [25]. In panel (b), the dashed colored lines show $\Delta \ln |E_N/B_2|$ where E_N/B_2 is calculated from Eq. (S3) with $\kappa = 1.448$.

the parameter $\alpha(N)$ as

$$\alpha(N) = -\frac{\pi C^2}{4} \frac{1}{\kappa |f_{\rm T}(0)|^2} \frac{B_2}{E_N} e^{\frac{4N}{C}}.$$
 (S4)

According to Ref. [8], $E_N = -B_2 e^{\frac{4N}{C} + c_1}$. Then

$$\alpha(N) = \alpha = \frac{\pi C^2}{4\kappa |f(0)|^2} e^{-c_1} \simeq 2.6073,$$
 (S5)

where we have used $f_{\rm T}(0)=2.207$, see, e.g., Ref. [7]. Results for $\alpha=2.6073$ are also presented in Fig. S1. In a more general approach,

$$E_N = -B_2 e^{\frac{4N}{C} + \theta(N)}, \tag{S6}$$

where $\theta(N) = \sum_{i=1} c_i N^{\gamma_i}$. Parameters c_i and γ_i may be fitted to the results of other methods, see Ref. [25] for an example of $\theta(N)$ fitted to the few-body limit results. Equation (S6) leads to the expression

$$\alpha(N) = \frac{\pi C^2}{4\kappa |f_{\rm T}(0)|^2} e^{-\theta(N)},\tag{S7}$$

where properly fitted $\theta(N)$ may improve the accuracy of generalized GPE in the few-body limit.

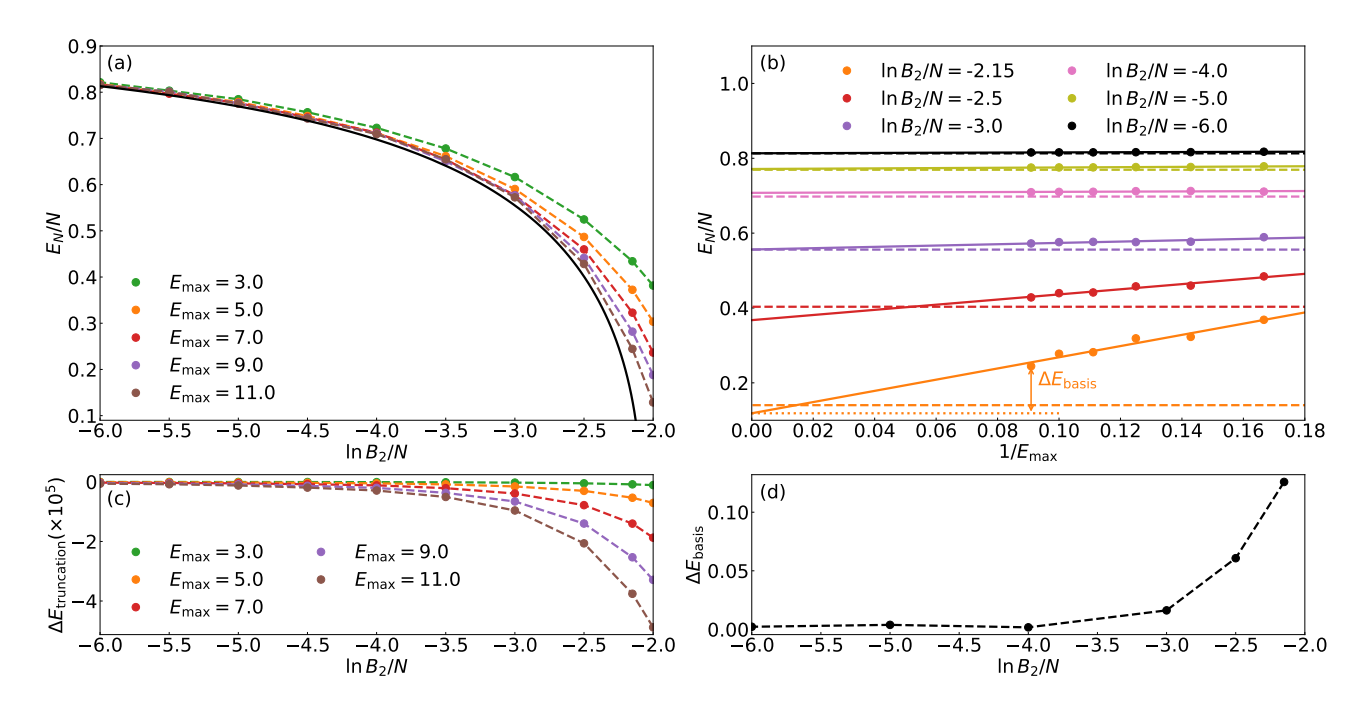


FIG. S2. The flow-equation approach for N=50. (a) Energy E_N as a function of interaction strength $\ln B_2/N$ for different basis sets parametrized by the maximal allowed energy, $E_{\rm max}$, (dots with dashed lines). The solid black curve shows the energy E_N calculated using Eq. (4) of the main text. (b) Energy E_N as a function of $1/E_{\rm max}$ for different $\ln B_2/N$ (dots). Solid lines show linear fit $a_1 + \frac{a_2}{E_{\rm max}}$. Dashed lines show energies E_N from Eq. (4). For $\ln B_2/N = -2.15$, we show how the error $\Delta E_{\rm basis}$ is calculated. (c) Truncation error $\Delta E_{\rm truncation}$ as a function of the interaction strength $\ln B_2/N$ for different $E_{\rm max}$. (d) Finite basis set error $\Delta E_{\rm basis}$ as a function of the interaction strength.

S2. THE FLOW EQUATION APPROACH (IM-SRG)

In this section, we discuss the general idea behind the flow-equation approach [31], also called the IM-SRG method [32]. For more details and previous applications to one-dimensional bosonic systems, see Refs. [33, 34, 47–49].

In the IM-SRG method, we block-diagonalize the Hamiltonian H in second quantization formalism using the flow equation

$$\frac{\mathrm{d}H}{\mathrm{d}s} = [\eta, H],\tag{S8}$$

where s is the flow parameter (which can also be understood as an imaginary time). With the proper choice of the generator of the flow η , the off-diagonal matrix elements will vanish in the $s \to \infty$ limit.

For our system, the Hamiltonian in the basis of non-interacting harmonic oscillator states $\{\psi_{(n_r,m)}\}$ is

$$H = \sum_{i} \epsilon_{i} a_{i}^{\dagger} a_{i} + \sum_{ijkl} B_{ijkl} a_{i}^{\dagger} a_{j}^{\dagger} a_{k} a_{l}, \quad (S9)$$

where the lower index denotes quantum numbers (n_r, m) with one-body energy $\epsilon_{(n_r,m)} = \hbar\omega(2n_r + |m| + 1)$ and

$$B_{ijkl} = \widetilde{g} \int d\mathbf{x} \psi_i(\mathbf{x}) \psi_j(\mathbf{x}) \psi_k(\mathbf{x}) \psi_l(\mathbf{x}), \qquad (S10)$$

where \widetilde{g} is the coupling constant.

The goal of the method is to decouple the ground state of the system from the rest of the Hilbert space. To achieve this, the Hamiltonian is transformed so that the system is expressed in terms of one- and two-body excitations relative to a chosen reference. In our case, the reference state is a non-interacting ground state, corresponding to the lowest-energy basis state $\psi_{(0,0)}$. Alternatively, one may employ a mean-field solution or construct it iteratively, updating the reference state after each flow step.

During the flow evolution, only one- and two-body operators are kept. The corresponding error $\Delta E_{\rm truncation}$ coming from discarding higher-order operators can be estimated using perturbation theory [33]. Moreover, the second type of error comes from a finite basis set. We limit the basis set to states $\psi_{(n_r,m)}$ with one-body energies $\epsilon_{(n_r,m)} < E_{\rm max}$. We fit the energies E_N for each interaction strength $\ln B_2/N$ to the function $a_1 + \frac{a_2}{E_{\rm max}}$ so that the energy $E_N \big|_{E_{\rm max} \to \infty} = a_1$. We estimate the error due to finite basis set as $\Delta E_{\rm basis} = \frac{1}{N} [E_N(E_{\rm max} = 11) - a_1]$.

In Figure S2, in panel (a), we show energies E_N for different sizes of the basis set as a function of $\ln B_2/N$. Panel (b) highlights the fitting procedure, showing E_N as a function of $E_{\rm max}$ together with the linear fit $a_1 + \frac{a_2}{E_{\rm max}}$. Panels (c) and (d) show errors coming from truncations

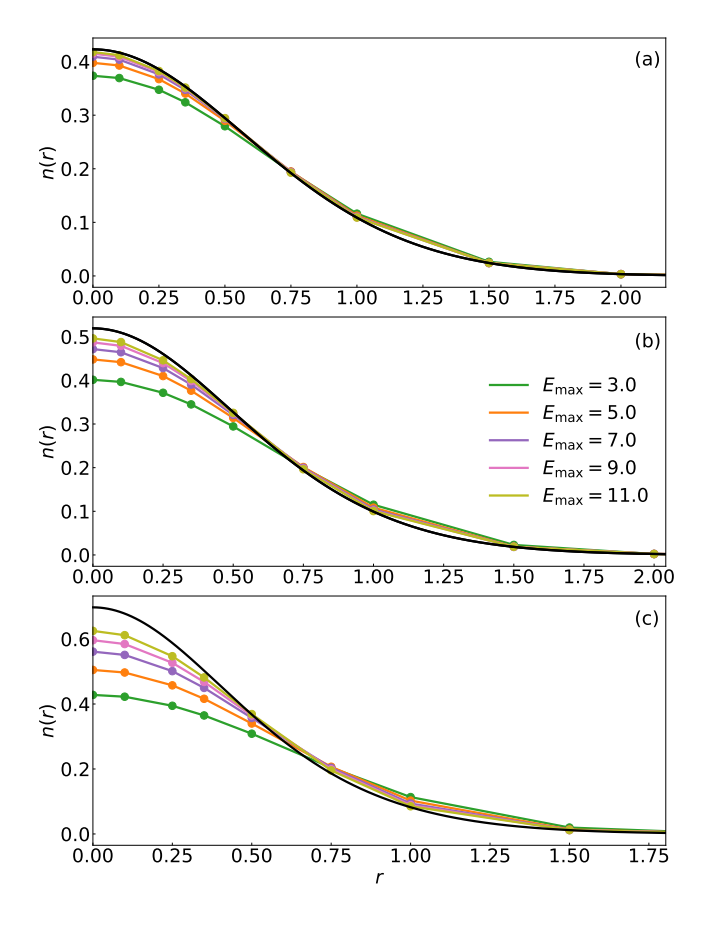


FIG. S3. Densities n(r) as a function of r for N=50 and $\ln B_2/N=$ (a) -6.0, (b) -4.0 and (c) -3.0. The dots with solid lines show results from the IM-SRG method with different $E_{\rm max}$. Solid black curves show densities calculated from Eq. (4).

during the flow evolution and from the finite basis set. Note that the truncation error is a few orders of magnitude smaller than the one coming from the finite basis set. For this reason, in Fig. 1 in the main text, we show only the value of $E_N=a_1$ with error bars given by $\Delta E_{\rm basis}$. Finally, Fig. S3, shows the ground-state density for different $E_{\rm max}$ compared to the densities calculated using Eq. (4) of the main text.

To compare IM-SRG results to GPE solutions, it is crucial to connect the interaction strength \widetilde{g} to the two-body binding energy B_2 . To do so, we calculate the lowest energy, E_2 of the two-body problem for different values of \widetilde{g} in a finite basis size. This provides us with the function $\widetilde{g}(E_{\max}, E_2)$. In IM-SRG calculations, we use $\widetilde{g}(E_{\max}, B_2)$, which fixes the lowest two-body binding energy to the correct value, see Ref. [50] for more details.

S3. NUMERICAL METHOD FOR GPE

In this section, we discuss the numerical method employed to solve Eq. (4) of the main text in the stationary and time-dependent versions.

Boundary conditions. We utilize the rotational symmetry of the problem and solve the equation for a radial function $f(r) = \sqrt{n(r)}$ on the spatial grid with size $N_{\rm g}+1$ with spacing dr, where we note $f_i \equiv f(r_i)$, and $r_i = idr$. For s=1, we expect that f(0)=0, which leads to the simple boundary condition $f_0=0$ with artificial points $f_{-1}=0$ and $f_{-2}=0$, ensuring proper treatment of the derivative terms within 4th order finite difference approximation. For s=0, we introduce boundary conditions $\frac{\partial f}{\partial r}\big|_{r=0}=0$ and $f(0)\neq 0$. To approximate the kinetic operator, we assume a symmetrical solution using artificial points $f_{-1}=f_1$, $f_{-2}=f_2$, and expand f(r) around r=0

$$f(r) \bigg|_{r \to 0} \approx f(0) + \frac{r^2}{2} \frac{\partial^2 f(r)}{\partial r^2} \bigg|_{r=0},$$
 (S11)

to properly address the kinetic operator at r_0 and r_1 . Additionally, for all s, we use boundary condition at $r \to \infty$ as $f \to 0$ by assuming that $f_{N_g+1} = 0$ and $f_{N_g+2} = 0$.

Ground-state calculations. To find the ground state of the system, we employ imaginary time evolution using a semi-explicit backward Euler scheme. This scheme is efficient for the imaginary-time evolution of non-linear GPE-like equations [51, 52]. After the change to imaginary time $t=i\tau$, the finite difference discretizations of the time derivative and application of the semi-explicit backward Euler scheme, we obtain an equation in the form

$$\left[\frac{1}{d\tau} + \hat{T} + W(r) + G[f^n]|f^n|^2\right]f^{n+1} = \frac{1}{d\tau}f^n, \quad (S12)$$

which is a linear matrix equation $\mathbb{A}\mathbf{v} = \mathbf{b}$, where \mathbb{A} is a sparse matrix, \mathbf{v} , \mathbf{b} are vectors; the superscript n denotes the timestep. In each imaginary timestep $d\tau$, we solve the above equation to find \mathbf{v} . The sparsity of the matrix \mathbb{A} allows us to employ efficient and robust Krylov solvers [53, 54].

Time evolution. For dynamics calculations, we solve the real-time evolution of the system. For this purpose, the backward Euler scheme cannot be used as it is not energy-conserving. Note that this property of the Euler scheme is actually beneficial for ground-state calculation, as the additional damping of the total energy increases the speed of the convergence. However, to simulate closed-system dynamics, we need to ensure that the total energy is conserved. For this purpose, we employ the Spectral Time Splitting Method [55].

Usually, in the Spectral Time Splitting Method, the kinetic operator is expressed in the momentum space using its Fourier transform. However, the standard form of this

numerical scheme ensures that the wavefunction vanishes at the system's edges. It is not straightforward to introduce the boundary condition $\frac{\partial f}{\partial r}\big|_{r=0}=0$ and $f(0)\neq 0$ in the Fourier space. Therefore, we treat the kinetic term in the position space as other operators. The main control parameter is energy error $\Delta E(t) =$ where $E_N(0)$ is the total energy of the initial state with post-quench Hamiltonian, and $E_N(t)$ is the total energy at time t. We consider our results as stable as long as $\Delta E(t) < 10^{-3}$. As we cannot ensure stability in longterm propagation, we perform a Fourier transform of the resulting signal only up to the time point at which the energy error is below the chosen limit, which may result in an unconverged Fourier spectrum. However, if for further investigation longer stable propagation is needed, the energy conservation error can be reduced by improving numerical methods, for instance, by calculating the evolution of the equation

$$i\frac{\partial \psi}{\partial t} = \left[-\frac{1}{2} \frac{\partial^2}{\partial \mathbf{x}^2} + W(\mathbf{x}) + GN|\psi|^2 - \mu(t) \right] \psi, \quad (S13)$$

where $\mu(t)$ is a chemical potential at time t. This scheme removes the trivial global phase associated with the stationary state [51, 56].

Dynamic grid approach. One of the main challenge of creating a robust computational scheme for our model are the different length scales of the solution depending on the interaction regime and number of bosons in the system. The size of the system $\langle r^2 \rangle$ can differ by several orders of magnitude from $\langle r^2 \rangle \simeq 1$ to even 10^{-20} . To ensure that our program is robust and does not require users to estimate the system's size, we introduce a dynamic grid approach. Every i-th time step, the program estimates the size of the intermediate state f^n , adjusts the calculation grid so $\frac{\sqrt{\langle r^2 \rangle}}{r_{N_{\rm g}-1}} \simeq 0.03$, and extrapolates f^n onto a new grid. We find that i=5 strikes a good balance between efficiently finding the proper grid size and keeping the overall computational cost low. This scheme ensures that we do not lose precision, that the state is well represented on the numerical grid, and that the system boundary at $r \to \infty$ does not introduce an artificial hardwall potential. We continue calculations until the relative changes between time steps are ΔE and $\Delta \langle r^2 \rangle < 10^{-8}$, where $\Delta O = \left| \frac{O^{n-1} - O^n}{O^n} \right|$, which ensures the convergence to the ground-state. However, while this scheme ensures that results are not dependent on the initial guess of the system size, good initial conditions dramatically accelerate convergence. To use that, we calculate the ground states in the sequence. First, we calculate the groundstate for weak interaction $\ln B_2/N$, for which the convergence is quick, and then we use the solution and its size as an initial state to calculate the ground state for $\ln B_2/N + \Delta(\ln B_2/N)$. Repeating this procedure with gradually increasing interaction strength allows us to ef-

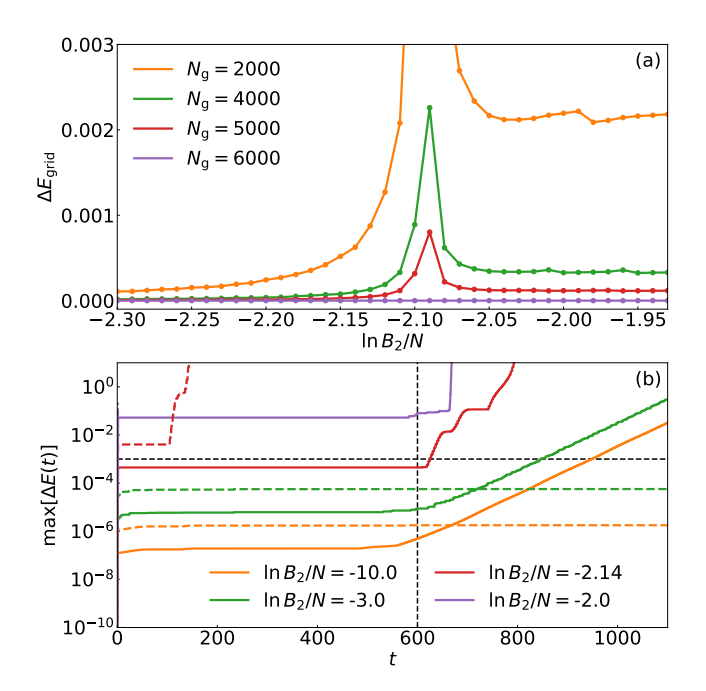


FIG. S4. (a) Relative energy error $\Delta E_{\rm grid} = |E(N_{\rm g}) - E(N_{\rm g} = 6000)|/|E(N_{\rm g} = 6000)|$ for ground-state calculation with N=50 as a function of the interaction strength, $\ln B_2/N$. The peak at $\ln B_2/N \simeq -2.1$ is an artifact due to E=0 at this point. (b) Maximal energy error $\max[\Delta E(t)]$ at time t for quench dynamics with N=50. Solid lines show results for $N_{\rm g}=6000$ and colored dashed lines for $N_{\rm g}=2000$. The black vertical line shows the cutoff t=600, which we use for $N_{\rm g}=6000$ to calculate the Fourier transform presented in Fig. 4 in the main text. Horizontal line $\max[\Delta E(t)]=0.001$ shows the limit above which we consider our result unstable.

ficiently calculate the ground state over the full range of interaction strengths.

Note that for real-time evolution, we do not employ the dynamic grid approach, as the extrapolation on the new grid introduces additional error. This error is not relevant for ground-state calculations, as the system evolves further towards the ground state after each grid adaptation. However, in the quench schemes that we consider, this is not a problem. In the collapse dynamics, the total energy of the initial harmonic state usually prevents the system from collapsing to sizes that cannot be adequately described by the initial grid (which is chosen with respect to the harmonic state). However, this limits our ability to perform quenches to stronger interactions above $\ln B_2/N > -2.14$, where we observe that the calculations become unstable even on short timescales. This suggests a potential area for improving our numerical method to handle changing length scales better during real-time evolution. In breathing-mode calculations, we use the grid obtained from the ground-state calculations, which is already fitted to describe the system at the relevant length scale. This is because we expect the breathing mode to be a weak oscillation around the equi-

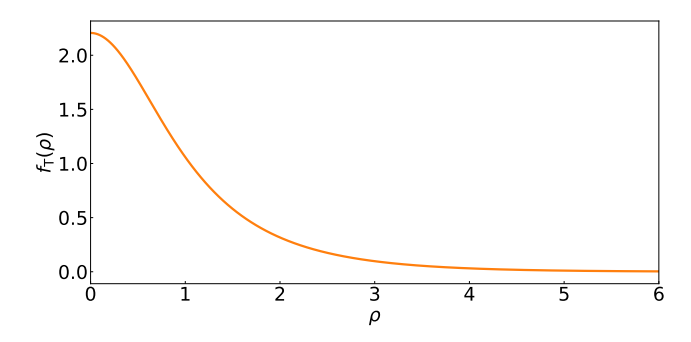


FIG. S5. Function $f_{\rm T}(\rho)$ determining the shape of the Townes soliton calculated as a solution of Eq. (S14).

librium state.

Computation parameters. For both ground-state calculations and dynamics, we use $N_{\rm g} = 6000$, which gives optimal accuracy and efficiency of the calculations. Panel (a) in Fig. S4, shows the relative error $\Delta E_{\rm grid} =$ $|E_N(N_g)-E_N(N_g=6000)|/|E_N(N_g=6000)|$ for N=50and for different interaction strengths $\ln B_2/N$. Note that at $\ln B_2/N \simeq -2.1$, the energy $E_N = 0$, which causes the relative error to suddenly increase without really affecting the accuracy of the calculations. For imaginary time evolution, we choose time step $d\tau = 0.1 dr$ and for real time evolution dt = 0.01dr. It is worth noting that decreasing the time step does not necessarily decrease accumulated energy error. For a timedependent scheme, the grid size $N_{\rm g}$ can directly and indirectly (through dt) affect the stability. We notice that for a smaller grid, the scheme is stable for a longer time tbecause it requires fewer time steps, but only for weaker interactions. For a larger grid, the overall energy error is lower, but the scheme becomes unstable in a shorter time t because more time steps are performed, which accumulate errors. For stronger interaction, both stability and error are better for larger grids. The panel (b) in Fig. S4 presents the maximal energy error $\max[\Delta E(t)]$ over time t for $N_{\rm g}=2000$ and $N_{\rm g}=6000$ with N=50, where $\max[\Delta E(t)]$ is defined as maximum value of $\Delta E(t)$ from the start of the propagation to time t.

The code in the Julia programming language that allows for the reproduction of all our results is available as an open-source program on GitLab [57].

S4. VARIATIONAL METHOD

To compute the lowest-energy solution of Eq. (4) from the main text variationally, we employ the scale-invariant Townes-soliton wavefunction [7] $\sqrt{n(r)} = (2\pi C\tilde{R}^2)^{-1/2} f_{\rm T}(r/\tilde{R})$, where $C \simeq 1.862$ and $f_{\rm T}(\rho)$ is a universal function satisfying equation

$$\frac{d^2 f_{\rm T}}{d\rho^2} + \frac{1}{\rho} \frac{df_{\rm T}}{d\rho} - f_{\rm T}(\rho) + f_{\rm T}^3(\rho) = 0.$$
 (S14)

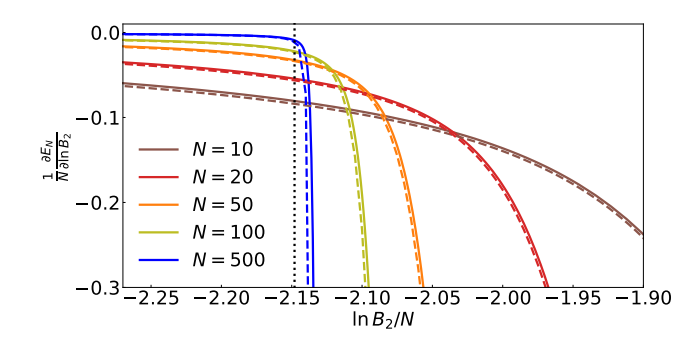


FIG. S6. Derivative of energy over the interaction strength $\frac{\partial E_N}{\partial \ln B_2}$ as a function of the interaction strength $\ln B_2/N$ for different number of bosons N. The solid curves show the exact numerical results; the dashed curves show the variational results with respect to the Townes-soliton profile. The vertical dotted line shows the transition point in the limit $N \to \infty$ [9, 10].

This function has a characteristic bell shape (see Fig. S5) with $f_{\rm T}(0) \simeq 2.206$ and $||f_{\rm T}|| = C$. The function $f_{\rm T}(\rho)$ can be found by solving Eq. (S14) using shooting method with boundary conditions $f_{\rm T}(\infty) = 0$ and $\frac{{\rm d}f_{\rm T}}{d\rho}\big|_{\rho=0} = 0$. This wavefunction has a single variational parameter, \tilde{R} , that determines the droplet's size; we numerically find the value of \tilde{R} that minimizes the energy E_N from Eq. (2). Results of this variational treatment are shown in Figs. 2 and S6.

The variational approach outlined here performs well across all interaction strengths because the Townessoliton profile is exact in the strong-interaction limit and provides a reasonable description of the ground state in the weakly interacting regime. [A comparison between the Townes profile and the non-interacting harmonic oscillator wavefunction is shown in Fig. 2.].

S5. DERIVATIVE OF THE ENERGY

Figure S6 shows the derivative of the energy E_N over the interaction strength $\ln B_2/N$. The derivative is smooth across the transition; however, it is expected to diverge to $-\infty$ for $N \to \infty$ at the transition point $\ln B_2/N \simeq -2.15$.

S6. BREATHING DYNAMICS

Similar to the standard mean-field description (see, e.g., [4]), the generalized Gross-Pitaevski equation leads to the continuity equation

$$\frac{\partial n}{\partial t} + \operatorname{div} \boldsymbol{j} = 0, \tag{S15}$$

where $\mathbf{j} = -\frac{i}{2}(\psi^* \nabla \psi - \psi \nabla \psi^*)$, $n = |\psi|^2$, and the equation for the evolution of momentum

$$\frac{\partial \mathbf{j}}{\partial t} = -\frac{1}{2} \nabla \left(\psi^* T \psi + \psi T \psi^* + \nabla \psi^* \nabla \psi \right)$$

$$- n \nabla \left[W + G N n \right],$$
(S16)

where T is the kinetic-energy operator.

Let us calculate the time evolution of the size of the system, $R^2 = \langle r^2 \rangle$. Using the continuity equation, we derive

$$\frac{\mathrm{d}R^2}{\mathrm{d}t} = 2 \int \mathbf{x} \mathbf{j} \mathrm{d}\mathbf{x}.$$
 (S17)

Differentiating this expression in time and using the equation for the evolution of momentum, we compute

$$\frac{\mathrm{d}^2 R^2}{\mathrm{d}t^2} = 4\langle T \rangle - 2\langle \mathbf{x} \nabla [W + GNn] \rangle, \tag{S18}$$

where $\langle T \rangle = E_{\rm kin}/N$ is a kinetic energy per particle. For a harmonic oscillator potential, this equation can be further rewritten as

$$\frac{\mathrm{d}^2 \langle r^2 \rangle}{\mathrm{d}t^2} = 4 \frac{E_N}{N} - 4R^2 - 2\langle \mathbf{x} \nabla G N n \rangle - 2\langle g N n \rangle. \quad (S19)$$

The last two terms do not cancel each other because of the broken scale invariance of the problem. This equation leads to Eq. (5) from the main text $(N \gg 1)$

$$\frac{\mathrm{d}^2 R^2}{\mathrm{d}t^2} = 4 \frac{E_N}{N} - 4R^2 + 2N \left\langle n^2 \frac{\mathrm{d}g}{\mathrm{d}n} \right\rangle. \tag{S20}$$

For the breathing dynamics, we assume that the solution has the form $\psi(r/R(t))/R(t)$. The time dynamics of R(t) reads

$$\ddot{R}^{2}(t) = \frac{4E_{N}}{N} - 4R^{2}(t) + \frac{N}{2\pi} \langle ng^{2} \rangle.$$
 (S21)

For small oscillations $R = R_0 + \delta R$, where $R_0 = R(t = 0)$ and $\delta R/R_0 \ll 1$, therefore, we can re-write this equation as

$$2R_0\delta\ddot{R}(t) \simeq -8R_0\delta R - \frac{N\delta R}{\pi R_0} \langle ng^2 \rangle_{t=0}.$$
 (S22)

The frequency of breathing oscillations is therefore

$$\Omega = \sqrt{4 + \frac{N}{2\pi R_0^2} \langle ng^2 \rangle_{t=0}}.$$
 (S23)

To arrive at the expression presented in the main text, note that $\langle ng^2 \rangle_{t=0} = 8\pi (R_0^2 - E_N/N)/N$.